Journal of Power Sources 195 (2010) 872–876

Contents lists available at ScienceDirect

Journal of Power Sources

journal homepage: www.elsevier.com/locate/jpowsour

Short communication

# Thermal diffusivity study of aged Li-ion batteries using flash method

Shrikant C. Nagpure[a,d,*], Ralph Dinwiddie[b], S.S. Babu[c], Giorgio Rizzoni[a], Bharat Bhushan[d], Tim Frech[e]

[a] Center for Automotive Research (CAR), The Ohio State University, 930 Kinnear Rd., Columbus, OH 43212, USA
[b] Oak Ridge National Lab (ORNL), One Bethel Valley Road, Bldg 4515, Oak Ridge, TN 37831, USA
[c] Integrated Systems Engineering, The Ohio State University, 1248 Arthur E Adams Drive, Columbus, OH 43210, USA
[d] Nanoprobe Laboratory for Bio- & Nanotechnology and Biomimetics (NLBB), The Ohio State University, 201 W. 19th Ave., Columbus, OH 43210, USA
[e] Edison Welding Institute (EWI), 1250 Arthur E Adams Drive, Columbus, OH 43221, USA

ARTICLE INFO

*Article history:*
Received 14 July 2009
Received in revised form 6 August 2009
Accepted 11 August 2009
Available online 19 August 2009

*Keywords:*
Li-ion
Battery aging
Infrared thermography
Flash method
Electric vehicles (EV)
Thermal diffusivity

ABSTRACT

Advanced Li-ion batteries with high energy and power density are fast approaching compatibility with automotive demands. While the mechanism of operation of these batteries is well understood, the aging mechanisms are still under investigation. Investigation of aging mechanisms in Li-ion batteries becomes very challenging, as aging does not occur due to a single process, but because of multiple physical processes occurring at the same time in a cascading manner. As the current characterization techniques such as Raman spectroscopy, X-ray diffraction, and atomic force microscopy are used independent of each other they do not provide a comprehensive understanding of material degradation at different length ($nm^2$ to $m^2$) scales. Thus to relate the damage mechanisms of the cathode at mm length scale to micro/nanoscale, data at an intermediate length scale is needed. As such, we demonstrate here the use of thermal diffusivity analysis by flash method to bridge the gap between different length scales. In this paper we present the thermal diffusivity analysis of an unaged and aged cell. Thermal diffusivity analysis maps the damage to the cathode samples at millimeter scale lengths. Based on these maps we also propose a mechanism leading to the increase of the thermal diffusivity as the cells are aged.


## 1. Introduction

Since its introduction in 1991, Li-ion battery technology has been growing and gaining popularity at a rapid pace. Advanced Li-ion batteries with high energy and power density are fast approaching compatibility with automotive demands. According to USABC, a 42 V battery in a hybrid electric vehicle (HEV) should have a calendar life of 15 years [1]. Electric vehicles (EV) should have a battery system that can last for 10 years [2]. In terms of cycles, 1000 cycles at 80% depth of discharge are expected in EV [2], and 300,000 cycles at 50 Wh are expected in a plug-in HEV [3]. However, the capacity (range) and power (performance) capabilities of these batteries decrease when subjected to the harsh duty cycles (current levels, low state of charge (SoC), depth of discharge (DoD), temperature profiles) of automobiles. This degradation or "aging" is a result of several simultaneous physiochemical processes that occur within the electrode, electrode-electrolyte interface, and within the electrolyte.

The aging mechanisms for the anode, cathode, and electrolyte are different from each other [4]. Investigation of aging mechanisms in lithium-ion batteries becomes very challenging, as aging does not occur due to a single process, but because of multiple physical processes occurring at the same time in a cascading manner. These cascading effects that lead to the aging of the cathode should be addressed by characterization of the nanomaterials used in this battery technology. Currently, characterization techniques such as Raman spectroscopy, X-ray diffraction (XRD), and atomic force microscopy (AFM) are used independent of each other to understand the degradation mechanisms. As a result, these studies do not provide a comprehensive understanding of material degradation at different length ($nm^2$ to $m^2$) scales. In addition, data is generally taken only on unaged and partially aged samples rather than at various degrees of aging. This lack of data at various length scales, as well as at various stages during aging, limits the development of phenomenological (electrochemistry, material) and functional models for battery life and performance estimation. In a cylindrical Li-ion battery a long strip of cathode, anode, and separator is rolled and packed in a can along with the electrolyte. Aging can occur uniformly or randomly over the long cathode strip. Since the cathode is made up of nanoparticles the material degradation will span nanometer to millimeter scale lengths. Thus, there is a need to identify the potential regions ($\mu m^2$) of material degradation within a large cathode area ($m^2$) to bridge the gap between

* Corresponding author at: Center for Automotive Research (CAR), The Ohio State University, 930 Kinnear Rd., Columbus, OH 43210, USA. Tel.: +1 614 432 3543; fax: +1 614 688 4111.
*E-mail address:* nagpure.1@osu.edu (S.C. Nagpure).

0378-7753/$ – see front matter © 2009 Elsevier B.V. All rights reserved.
doi:10.1016/j.jpowsour.2009.08.025

the $m^2$ and $nm^2$ to $\mu m^2$ scale lengths. A multiscale characterization of the cathode would present a complete understanding of the degradation mechanisms in the cathode. So, to completely understand the aging mechanisms in the cathode, we need to scan a large surface area of the cathode (on the order of 1 $m^2$) to identify early stages of material degradation in small regions (in the order of $1 \times 10^{-10}$ $m^2$). An exhaustive search over large area with different aging conditions will be physically impossible with available microscopic characterization techniques.

In this paper, for the first time we propose the use of thermal diffusivity study using the flash method to identify the material degradation areas in the cathode. It has been experimentally observed that the aging of Li-ion batteries leads to an increase in the internal resistance (power fade) and a decrease of capacity (charge acceptance) [5]. The rise in the internal resistance is directly related to the change in the electrical impedance of the battery components, such as the anode and the cathode. A change in the electrical impedance of the cathode occurs due to several physiochemical reactions. It is anticipated that the thermal resistivity may be a measure of the electrical impedance, and therefore thermal diffusivity analysis using a high-resolution thermography instrument will help in understanding the damage to the cathode samples at millimeter scale lengths. The maps generated with infrared (IR) thermal imaging will identify the aging distribution over the entire cathode surface. This will help in identifying whether the aging process is uniform over the cathode surface or if it occurs at certain preferential sites or regions of the cathode. Using 2D thermography maps, test samples from a specific area can be prepared for further micro/nanocharacterization. Thus thermal imaging will bridge the gap between the macrolevel and micro/nanolevel characterization of the cathode material. This technique can also be used at the manufacturing stage to identify any defects that may be occurring while laying the active cathode material on the aluminum substrate. We present the thermal diffusivity analysis conducted on a lithium iron phosphate ($LiFePO_4$) cathode extracted from an unaged cell and an aged cell. The results of our study indicate an increase in the thermal diffusivity of the cathode material as the cell is cycled. Based on our thermal diffusivity results, we have proposed a mechanism for heat diffusion through the cathode to the first order approximation.

## 2. Experimental details

### 2.1. Experimental setup

The setup to capture the thermal diffusivity maps of the samples is the same as discussed in ASTM – 1461 92 standard [6] and is shown in Fig. 1. The main features of this setup are the flash lamp, sample mount, high-resolution IR camera, and data acquisition system. The high energy pulse required in this experiment is generated by Profoto, Acute 2, flash lamp with a 2400 W s capacity. The flash lamp is operated to deliver a finite pulse of energy at 300 W s. The sample mount is a custom made hollow box with a square slot of approximately 63.5 mm × 63.5 mm on one face. The flash lamp is centered over this slot. A circular hole of approximately 90 mm is cut on the opposite face. The IR camera lens is inserted through this hole and focused on the sample. The thermal maps are taken with an IR camera from Indigo Systems, Phoenix Mid-wave IR Camera, with a 320 × 256 pixel resolution and InSb focal plane array. The frequency of the camera is set at 346 Hz. The data acquisition system is built into the IR camera equipment.

The sample is mounted flushed on the face with the square slot on the sample mount. The center of the flash lamp coincides approximately with the center of the sample so that the heat pulse

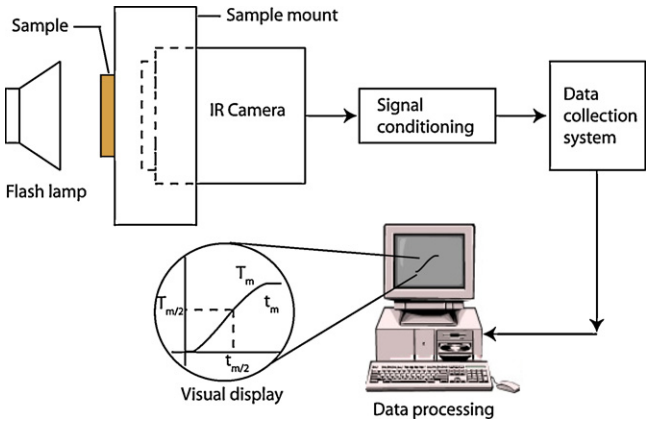


**Fig. 1.** Schematic of thermal diffusivity measurement by flash method (adapted from [9]).

is uniformly incident on the sample. The IR camera lens is focused on the opposite face of the sample with the center of the lens aligned approximately with the center of the sample. The finite heat pulse from the flash lamp is incident on the front face of the sample. The heat gained by the sample from this pulse is conducted through its thickness to the rear face. As such the rear face of the sample is heated and its temperature increases. It is important to note that the temperature rise in the samples is only in the order of few degrees above or below the ambient temperature. The IR camera captures this heat gained by the rear face at a frequency of 346 frames per second. The experimental setup was under ambient conditions and as such all the thermal maps were obtained under ambient conditions.

### 2.2. Sample preparation

The cylindrical Li-ion batteries used in these experiments have a graphite anode and a cathode made of $LiFePO_4$ nanoparticles (40–50 nm). Graphite is bonded onto a copper substrate, and $LiFePO_4$ nanoparticles are bonded onto an aluminum substrate using a polyvinylidene difluoride binder (PVDF). The anode and the cathode, with a separator in between, are rolled and then packed in a can to form a cylindrical cell. The electrolyte used in this cell is a lithium hexafluorophosphate ($LiPF_6$) salt in alkylene carbonates. The cell has an operating voltage of 3.3 V and a nominal discharge capacity of 2.3 Ah. The $LiFePO_4$ nanoparticles have very poor conductivity ($\sigma = 2 \times 10^{-9}$ S $cm^{-1}$) [7,8], and hence to increase their conductivity, they are coated with carbon [9]. Two such batteries with the same capacity are chosen for this study. One of the batteries is cycled only once through the capacity test to measure its capacity and is labeled as an unaged cell. The other cell is cycled at a rate of 16C[1] at 50% SoC and ±5% DoD until the cell reached its end of life (EOL) and is labeled as an aged cell. The cell was cycled for 33,600 cycles before it reached its EOL. According to the automobile industry, a cell is said to have reached its EOL if the capacity degrades by 20% of its original capacity [2]. The batteries were then disassembled, and the long cathode strip was extracted from the cell and unrolled. The entire cathode was divided into five equal sections as shown in the schematic Fig. 2a. Section 1 is closer to the outside of the cylinder while section 5 is towards the center of the cylinder. Each section is approximately 63.5 mm × 63.5 mm. The thermal maps were obtained over these five sections of the aged and the unaged cathode.

[1] 1C = 2.3 Ah.

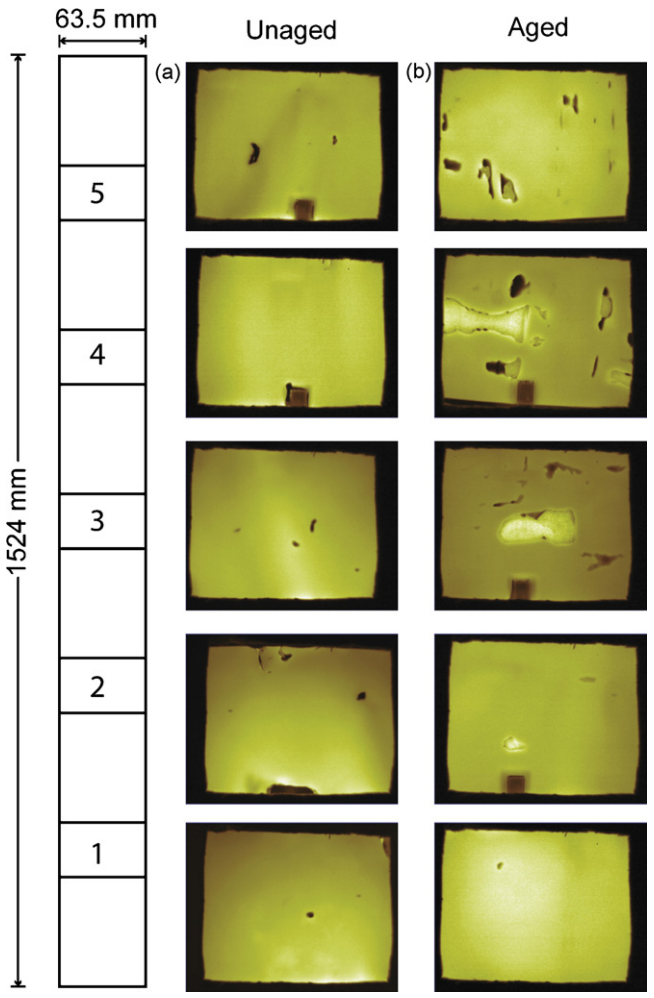


**Fig. 2.** (a) Sectioning of the cathode for the thermal imaging. Section 1 is near the core of the cylinder and section 5 is near the out edge of the cylinder. (b) Thermal maps of unaged and aged cathode samples for all the five sections.

## 3. Results and discussion

The thermal maps of the aged and unaged sample for all five sections, shown in Fig. 2b, are taken when the temperature of the rear face of the sample reaches the maximum value. In these thermal maps the dark spots represent the cold areas while the bright spots represent the hot area. The dark spots are more prominent in the aged sample (right side) as compared to the unaged sample (left side). This indicates that the aged sample is conducting the heat received from the flash lamp much faster than the unaged sample. Also the dark spots occur randomly over the sample surface. This indicates that the aging occurs non-uniformly over the cathode surface. In order to quantify this behavior in terms of thermal diffusivity the following analyses was performed.

Fig. 3 shows the temperature rise of the rear face of the sample in terms of IR counts. The temperature rise shown here is for section 4 of the aged and the unaged cathode samples shown in Fig. 2b. An area with a uniform IR intensity is randomly chosen in the thermal map of the aged and unaged sample for thermal diffusivity analyses. The IR counts are obtained over this area from the instant the heat pulse is incident on the sample until the temperature of the sample reaches a steady state value. A base line temperature is identified in these plots as the temperature just before the pulse is incident on the sample ($T_{ini}$). Then the maximum temperature is measured as the steady state temperature of the rear face of the sample ($T_{max}$). The half rise time ($t_{1/2}$), i.e. the time required from the initiation of

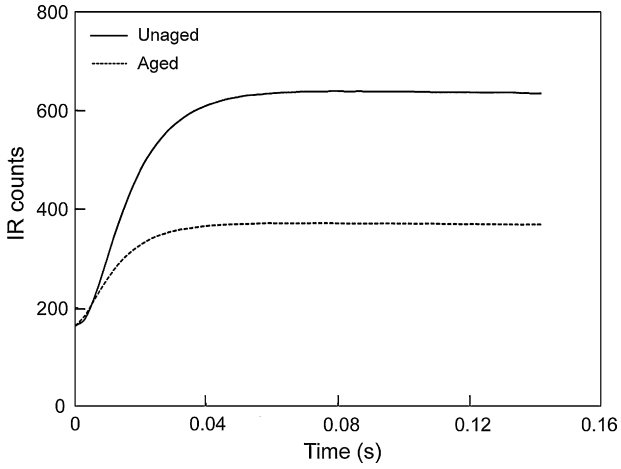


**Fig. 3.** Temperature rise curves for unaged and aged samples (section 4).

the pulse on the front face of the sample to the time at which the temperature of the rear face of the sample reached half the difference between $T_{ini}$ and $T_{max}$, is calculated. The thermal diffusivity for the sample is then calculated using the following formula [9]:

$$\alpha = 0.13879\frac{L^2}{t_{1/2}} \quad (1)$$

where $\alpha$ is the thermal diffusivity ($m^2\ s^{-1}$), $L$ is the thickness of the sample (m), and $t_{1/2}$ is the half rise time (s). It is important to note that the Eq. (1) is not dependent on the absolute value of $T_{max}$. Therefore, the observed differences in maximum IR counts between aged and unaged samples as seen in Fig. 3 are not important in these analyses.

Fig. 4 compares the thermal diffusivity between the unaged and the aged sample over all the five sections. As can be seen in this figure the thermal diffusivity of the aged sample is more than the unaged sample in all the five sections. The differences in the thermal diffusivity values between aged and unaged samples are significantly less in sections 1 and 5. These sections are near the core of the cylinder and near the outer edge of the cylinder, respectively. The differences in the thermal diffusivity are more prominent in sections 2–4 of the samples. It is believed that the different rate of change in the porosity in various sections leads to the non-uniform change in the thermal diffusivity across the sections. The effect of porosity on the thermal diffusivity of the samples has been discussed later. Theoretically, thermal diffusivity is given as the ratio

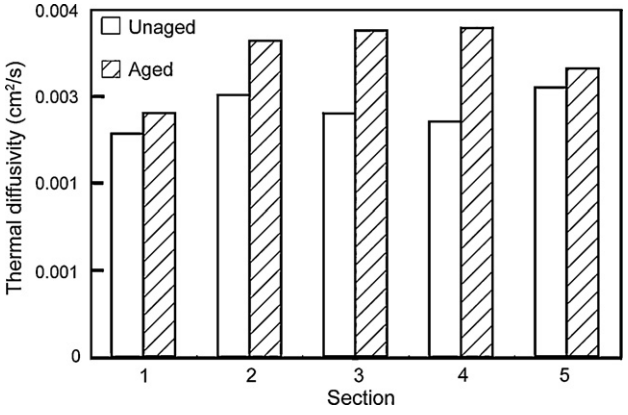


**Fig. 4.** Comparison of thermal diffusivity between unaged and aged samples.

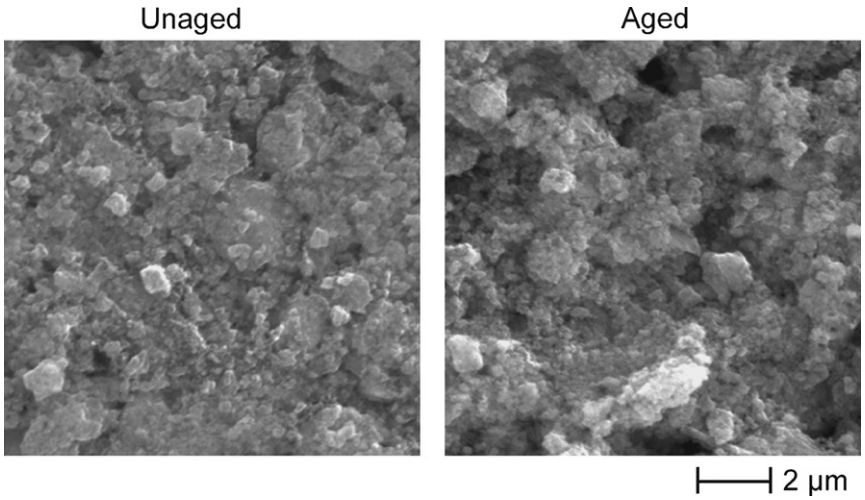


**Fig. 5.** SEM micrographs of unaged and aged cathode samples extracted from section 4.

of the thermal conductivity to volumetric heat capacity as follows:

$$\alpha = \frac{k}{\rho c_p} \tag{2}$$

where $\alpha$ is the thermal diffusivity ($m^2\,s^{-1}$), k is the thermal conductivity ($W\,m^{-1}\,K^{-1}$), and $\rho c_p$ is the volumetric heat capacity ($J\,m^{-3}\,K^{-1}$). The Eq. (2) is strictly applicable only to monolithic material. In our case, the cathode material is a composite, and an increase in $\alpha$ can be associated with a change in $k$, $\rho$ and/or $c_p$.

To investigate the mechanism for increase in the thermal diffusivity, SEM micrographs of the unaged and aged samples were obtained (Fig. 5). The SEM micrographs reveal the coarsening of the nanoparticles in the aged samples as compared to the unaged sample. The particles in the unaged sample are of the order 40–50 nm while in the aged sample the particles are of the order 240–350 nm. The coarsening of the particles leads to a decrease in the effective surface area of the particles. The coarsening phenomenon can also lead to the disbonding of these particles from the aluminum substrate. In addition to this, Kostecki and McLarnon [10] have also observed nanocrystalline deposits (NCD) formed on $LiNi_{0.8}Co_{0.2}O_2$ cathode surface due to the secondary chemical reactions.

In our previous work [11], we have discussed the effect of grain coarsening and NCD on the surface electrical resistance of the cathode (Fig. 6). As shown in the schematic the resistance of the $LiFePO_4$ cathode surface increases as the cells are cycled because of the coarsening. The coarsening also causes loss of the carbon coating which leads to the further increase in the surface electrical resistance of these particles. In addition to this, the total surface resistance of the aged sample increases due to the additional electrical resistance from NCD. The above surface electrical resistance measurements may appear to be contradictory to the current thermal diffusivity measurements. However, thermal diffusivity measurements are sensitive to physical processes that occur in thickness direction.

Based on the thermal diffusivity experimental results, we propose a first order approximate heat conduction mechanism as the cathode ages and its surface resistance increases due to cycling. Fig. 7 shows the schematic of a proposed mechanism explaining the increase in the thermal diffusivity of a $LiFePO_4$ cathode due to aging. As a first order approximation the cathode can be considered as a porous medium. Also, it can be assumed here that the heat diffuses through the cathode only due to conduction. As the cathode ages the nanoparticles tend to coarsen (Fig. 5) by sintering. Due to this sintering of the nanoparticles, the effective surface area per unit volume decreases [12], with an associated decrease in the porosity

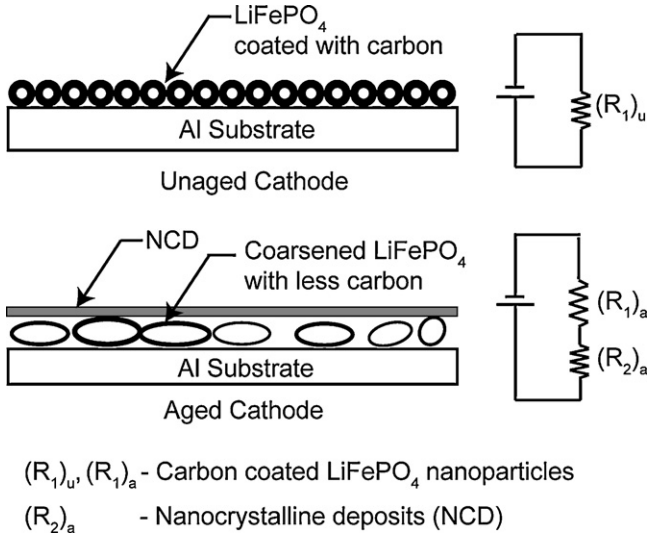


**Fig. 6.** Schematic of a proposed mechanism explaining increase in the surface resistance of a $LiFePO_4$ cathode due to aging [11].

of the cathode. It is interesting to note that the sintering of oxide particles takes place at high temperatures. The onset of sintering in the cathode material may be attributed to the high surface energy of the $LiFePO_4$ nanoparticles. Zhang and Miser [13] have observed coalescence of oxide particles with no external heating. In general,

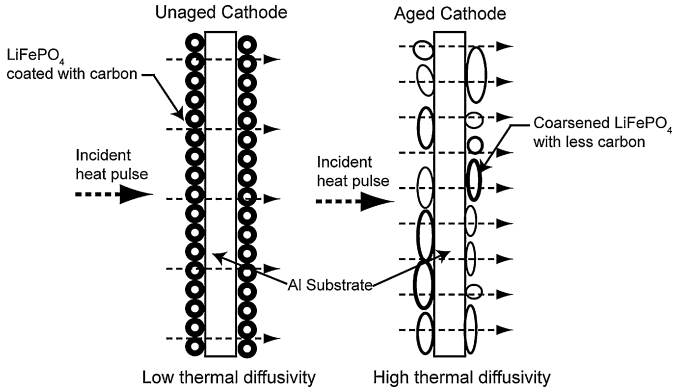


**Fig. 7.** Schematic of a proposed mechanism explaining increase in the thermal diffusivity of a $LiFePO_4$ cathode due to aging.

as the porosity of the medium decreases, the thermal conductivity increases, and hence, the aged sample shows increase in thermal diffusivity [14,15].

The effect of the NCD shown in Fig. 6 can be neglected in this mechanism as the thickness of the NCD would be negligible (50–200 nm in case of $LiNi_{0.8}Co_{0.2}O_2$ cathode [16]) as compared to the thickness of the cathode surface. A small decrease in thermal diffusivity due to NCD will be below the resolution of the current measurement technique. In addition, due to coarsening and subsequent disbonding of the nanoparticles from the aluminum substrate, the substrate will be exposed to the incident heat pulse directly. Since aluminum has high thermal diffusivity ($8.418 \times 10^{-5}\ m^2\ s^{-1}$), the overall thermal diffusivity of the aged sample may show an apparent increase [17,18,19]. The presence of many dark spots (see Fig. 2) is supportive of this hypothesis. The above results demonstrate that 2D thermography measurements can be used to identify the onset of aging in large surface area typical to that of commercial batteries.

## 4. Conclusion

In this paper, thermal diffusivity analysis by flash method is shown to be an effective technique to map the damage of the cathode in Li-ion batteries at millimeter length scales.

Thermal diffusivity bridges the gap between different length scales and proves to be an effective technique to relate the damage mechanisms of the cathode at mm length scale to micro/nanoscale. The 2D thermography maps generated in this study demonstrate that the damage occurs randomly over the cathode surface and has no preferential sites. Also, the thermal diffusivity increases as the cathode ages during the cycling of the batteries. The increase in the thermal diffusivity is attributed to the decreased porosity of the cathode samples due to the coarsening of the $LiFePO_4$ nanoparticles.

## Acknowledgments

The authors would like to thank Institute of Materials Research (IMR) at The Ohio State University, for the financial support of this work. This research at the Oak Ridge National Laboratory's High Temperature Materials Laboratory was sponsored by the U. S. Department of Energy, Office of Energy Efficiency and Renewable Energy, Vehicle Technologies Program. The authors would like to express their sincere gratitude towards Dr. Sandip Mazumder for his valuable inputs. The authors would also like to thank Dr. Yann Guezennec and John Neal of CAR, The Ohio State University for their help in acquiring the cells and managing their aging under controlled conditions.

## References

[1] Anonymous, FreedomCAR 42V Energy Storage System End-of-Life Performance Goals, USABC, Southfield, MI, 2002, available from http://www.uscar.org/guest/view_team.php?teams_id=12.
[2] Anonymous, USABC Goals for Advanced Batteries for EVs, USABC, Southfield, MI, 2006, available from http://www.uscar.org/guest/view_team.php?teams_id=12.
[3] Anonymous, USABC Requirements of End of Life Energy Storage Systems for PHEVs, USABC, Southfield, MI, 2006, available from http://www.uscar.org/guest/view_team.php?teams_id=12.
[4] J. Vetter, P. Novák, M.R. Wagner, C. Veit, K.C. Möller, J.O. Besenhard, M. Winter, M. Wohlfahrt-Mehrens, C. Vogler, A. Hammouche, J. Power Sources 147 (2005) 269–281.
[5] Z. Chehab, L. Serrao, Y. Guezennec, G. Rizzoni, Proceedings of the 2006 ASME International Mechanical Engineering Congress and Exposition, 2006.
[6] Anonymous, Standard Test Method for Thermal Diffusivity of Solids by the Flash Method, 1992, ASTM Designation: E 1461–92.
[7] S. Franger, F. Le Cras, C. Bourbon, C. Benoit, P. Soudan, J. Santos-Penã, in: S.G. Pandalai (Ed.), Recent Research Developments in Electrochemistry, vol. 8, Transworld Research Network, Kerala, 2005, pp. 225–256.
[8] C. Benoit, S. Franger, J. Solid State Electrochem. 12 (7–8) (2008) 987–993.
[9] J.B. Goodenough, J. Power Sources 174 (2007) 996–1000.
[10] R. Kostecki, F. McLarnon, Electrochem. Solid State Lett. 5 (7) (2002) A164–A166.
[11] S.C. Nagpure, B. Bhushan, S. Babu, G. Rizzoni, Scripta Mater. 60 (2009) 933–936.
[12] H.E. Exner, E. Arzt, in: R.W. Cahn, P. Haasen (Eds.), Physical Metallurgy, 3rd and revised ed., Elsevier Science Publication, 1983, Chapter 30.
[13] W.J. Zhang, D.E. Miser, Coalescence of Oxide Nanoparticles: In situ HRTEM Observation, J. Nanopart. Res. 8 (6) (2006) 1027–1032.
[14] V.I. Kononenko, V.M. Baranovskii, V.P. Dushchenko, Powder Metall. Metal Ceram. **7** (3) (1968) 175–177.
[15] A. Bhattacharya, V.V. Calmidi, R.L. Mahajan, Int. J. Heat Mass Transfer 45 (2002) 1017–1031.
[16] X. Zhang, P.N. Ross Jr., R. Kostecki, F. Kong, S. Sloop, J.B. Kerr, K. Striebel, E.J. Cairns, F. McLarnon, J. Electrochem. Soc. 148 (2001) A463–A470.
[17] A.I. Brown, S.M. Marco, Introduction to Heat Transfer, 3rd ed., McGraw-Hill, 1958.
[18] E.R. Eckert, R.M. Drake, Heat and Mass Transfer, McGraw-Hill, 1959.
[19] J.P. Holman, Heat Transfer, 9th ed., McGraw-Hill, 2002.